

Signatures of Rapidly Rotating Stars with Chemically Homogeneous Evolution in the First Galaxies

BOYUAN LIU ¹, YVES SIBONY ², GEORGES MEYNET ² AND VOLKER BROMM ^{3,4}

¹*Institut für Theoretische Astrophysik, Zentrum für Astronomie, Universität Heidelberg, D-69120 Heidelberg, Germany*

²*Department of Astronomy, University of Geneva, Chemin Pegasi 51, 1290 Versoix, Switzerland*

³*Department of Astronomy, University of Texas at Austin, 2515 Speedway, Stop C1400, Austin, TX 78712, USA*

⁴*Weinberg Institute for Theoretical Physics, University of Texas at Austin, Austin, TX 78712, USA*

ABSTRACT

The James Webb Space Telescope (*JWST*) has revealed an unexpectedly high abundance of UV luminous galaxies at redshifts $z \gtrsim 10$, challenging ‘standard’ galaxy formation models. This study investigates the role of rapidly rotating (massive) stars undergoing chemically homogeneous evolution (CHE) in reconciling this potential tension. These stars are more compact, hotter, and exhibit enhanced UV emission. We find that the rest-frame UV luminosity of star-forming galaxies can be significantly enhanced by a factor of $\sim 3 - 6$ when CHE stars above a minimum initial mass of $m_{*,\min}^{\text{CHE}} \sim 2 - 10 M_{\odot}$ account for more than half of the total stellar mass following a Salpeter initial mass function. As a result, the UV luminosity functions observed at $z \sim 12 - 16$ can be reproduced with less extreme values of star formation efficiency and UV luminosity stochastic variability. Our results highlight the potential of CHE in explaining the UV-bright galaxy populations detected by *JWST* and call for future work to explore the broader astrophysical implications of CHE and its associated phenomena in the early universe, such as gamma-ray bursts, compact object binaries, and metal enrichment.

Keywords: Population III stars (1285) – Population II stars (1284) – High-redshift galaxies (734) — James Webb Space Telescope (2291) — Early universe (435) – Stellar evolution (1599)

1. INTRODUCTION

Early results from the *JWST* have challenged the standard model of galaxy formation in the high- z universe (Boylan-Kolchin 2023), with the discovery of a surprising abundance of UV bright galaxies at $z \gtrsim 10$ (e.g., Finkelstein et al. 2023, 2024; Labbé et al. 2023; Adams et al. 2024; Donnan et al. 2024). Two broad classes of explanations have been discussed, modifications to the underlying Λ CDM model of cosmological structure formation (e.g., Liu & Bromm 2022; Shen et al. 2024), or models that vary assumptions in the standard picture of star formation. The second (baryonic) category explores scenarios that either increase the stellar mass/star formation rate in a given dark matter host halo, by boosting the star formation efficiency (SFE, e.g., Inayoshi et al. 2022; Dekel et al. 2023) or variability/burstiness of UV emission/star formation (e.g., Shen et al. 2023), or

those that enhance the stellar light-to-mass ratio¹. An example for the latter explores a top-heavy initial mass function (IMF; e.g., Cueto et al. 2024; Trinca et al. 2024; Ventura et al. 2024), as predicted for the metal-poor environments in the early universe (e.g., Liu et al. 2024).

Thus invoking a top-heavy IMF or an increased formation efficiency may, however, only boost star formation locally, but suppress it on galactic scales, by triggering disruptive stellar feedback, such as strong supernova (SN) activity (e.g., Jeong et al. 2024). Here we propose a different (baryonic) solution for the early UV-bright galaxy problem: The stellar light-to-mass ratio is boosted because of a population of stars that undergo chemically homogeneous stellar evolution (CHE), which become more compact and hotter than normal stars. Such CHE stage could be realized for rapidly rotating stars, where their structure adapts by triggering

Corresponding author: Boyuan Liu
Email: boyuan.liu@uni-heidelberg.de

¹ Alternatively, strong radiation-pressure driven outflows could remove UV dust attenuation during the early evolution of high- z galaxies (e.g., Ferrara 2024).

strong internal mixing currents (e.g., Maeder 1987; Yoon & Langer 2005; Cantiello et al. 2007; Yoon et al. 2012; Maeder & Meynet 2012; Song et al. 2016; Mandel & de Mink 2016; de Mink & Mandel 2016; Marchant et al. 2017; du Buisson et al. 2020; Riley et al. 2021). Rotation speeds close to the break-up value have been predicted for the first Population III (Pop III) stars, formed in the unique metal-free conditions² of dark matter mini-halos (Stacy et al. 2011, 2013). Similarly, metal-poor Population II (Pop II) stars may be able to retain their natal rotation speeds, because of their significantly reduced mass loss due to weakened radiatively-driven stellar winds (e.g., Vink et al. 2001). Recent direct observations of select O-type stars in nearby metal-poor dwarf galaxies suggest that stellar winds may be even weaker than what was previously predicted by theory (Gormaz-Matamala et al. 2024; Telford et al. 2024).

The impact of a CHE-boosted production of H, He, and possibly He⁺, ionizing radiation from Pop III stars on the early stages of reionization was explored in a previous study (Sibony et al. 2022), placing constraints on the fraction of Pop III stars that undergo CHE (see also Liu et al. in prep.). The reionization modeling, however, is subject to the uncertain escape fraction of ionizing radiation from the galaxy host halos, whereas any constraints from the non-ionizing UV continuum are more direct indications of the underlying stellar populations. We note that there have been recent indications for the metal enrichment from rapidly rotating stars in the first galaxies, inferred from their chemical abundance patterns with deep *JWST* spectroscopy. Prominent among them are high nitrogen-to-oxygen abundance ratios, e.g., in GN-z11 and RXCJ2248-ID (Bunker et al. 2023; Topping et al. 2024), which may be explained with models of rapidly rotating, massive stars (e.g., Tsiatsiou et al. 2024; Nandal et al. 2024). Another nucleosynthetic signature of rapidly rotating stars is the proposed boost in carbon production (Liu et al. 2021; Jeena et al. 2023), providing a possible explanation for strong carbon emission lines detected in $z \gtrsim 12$ galaxies (e.g., D’Eugenio et al. 2024) and carbon-enhanced extremely metal-poor stars in the Milky Way (e.g., Zepeda et al. 2023). We will therefore explore in the following whether a rapidly rotating subset of stars under CHE within the first galaxies can account for the emerging *JWST* phenomenology of UV bright galaxies in the first few hundred million years of cosmic history.

² Magnetic fields arising from dynamo activity in the primordial protostellar disks could complicate the situation, leading to a possible bifurcation into cases of rapid and slow rotation (Hirano & Bromm 2018).

2. CHEMICALLY HOMOGENEOUS EVOLUTION

2.1. Stellar Evolution

The stellar evolution models for stars evolving homogeneously are based on $n = 3$ polytropes with a time-varying mass fraction of hydrogen, as detailed in Sibony et al. (2022). In that work Pop III stars with initial masses (m_*) between 9 and 300 M_\odot were computed. Here we complement our previous grid by adding tracks for lower initial mass stars with masses between 1.7 and 7 M_\odot . As a comparison sample, we use the stellar tracks for non-rotating Pop III stars in the same mass range (1.7–300 M_\odot) from Murphy et al. (2021). Here, we only consider metal-free stellar evolution models for simplicity, while freely varying the IMF parameters (see Sec. 2.2 below). The difference in rest-frame UV ($\lambda \sim 1500 \text{ \AA}$) luminosity when changing the metallicity (from $Z = 0$ to 0.02) under a fixed Kroupa (2001) IMF is minor (within a factor of ~ 2) for a typical star formation timescale ~ 100 Myr, according to the Yggdrasil stellar population synthesis models (Zackrisson et al. 2011).

Homogeneous evolution requires that the timescale for chemical mixing is much smaller than the nuclear timescale during the Main-Sequence (MS) phase. The mixing timescale scales as R^2/D_{mix} , where R is the stellar radius, and D_{mix} the diffusion coefficient describing the transport of the chemical elements. Maeder & Meynet (2000, see their paragraph 3.1) showed that the ratio of the mixing timescale to MS lifetime approximately varies as $1/m_*$ for stars more massive than 15 M_\odot . This indicates that when the mass decreases, the mixing timescale increases faster than the MS lifetime. Thus, we can expect to reach a lower initial mass limit, $m_{*,\text{min}}^{\text{CHE}}$, below which homogeneous evolution will not be obtained. The precise limit depends on the initial rotation and metallicity, with lower values when the initial rotation increases and when the metallicity decreases (this is due at least in part to the fact that at lower metallicities, stars are more compact).

This limit also depends on the physics used for chemical mixing and for the transport of angular momentum. These two transport mechanisms are intimately related since the gradients of chemical composition impact angular momentum transfer, which in turn influences the transport of the chemical elements. For this work, since we do not use a peculiar physical mechanism to obtain the homogeneous tracks, we simply consider the value of this limit as a free parameter. Most of the stellar models computed so far have focused on the massive stellar range down to lower masses between 5 and 10 M_\odot (see e.g., Riley et al. 2021), so we may wonder if it is justified here to extend this limit further. As indicated

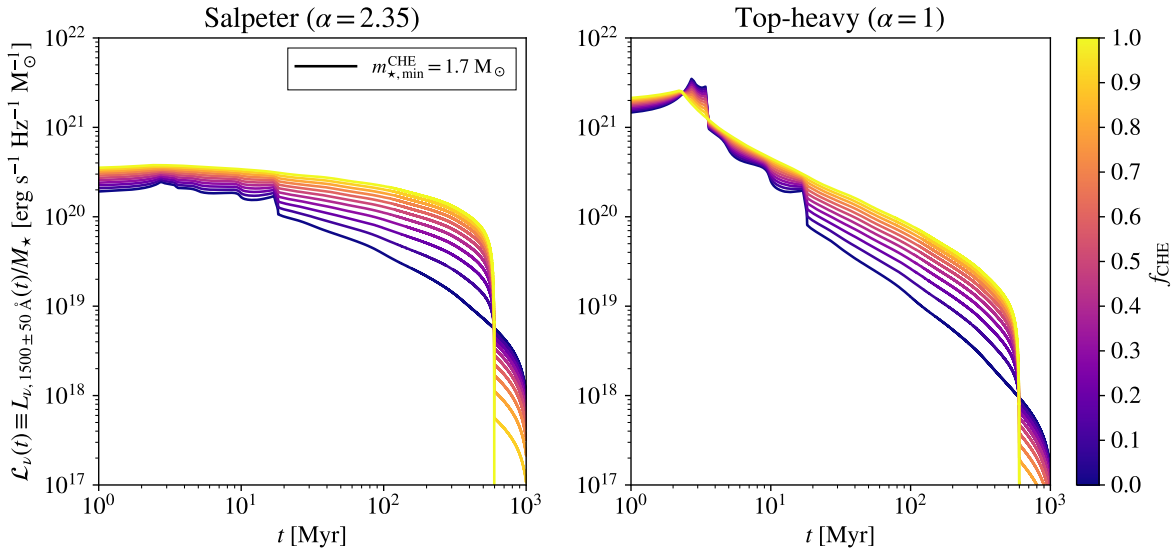


Figure 1. Rest-frame UV light curve: evolution of UV luminosity normalized by the total stellar mass for a single-age stellar population. The left (right) panel shows the results for a Salpeter (top-heavy) IMF, $dN/dm_* \propto m_*^{-\alpha}$, with a slope $\alpha = 2.35$ (1) and a mass range $m_* \in [1.7, 300] M_\odot$ for both normal and CHE stars. The mass fraction of CHE stars f_{CHE} is varied between 0 and 1, with lighter colors denoting larger f_{CHE} .

above, the limit depends on the physics of mixing which is still not yet fully understood. On the other hand, fast rotation is likely not the only process that may lead to homogeneous stars. For instance, grazing collisions have been found to result in nearly completely mixed stars producing blue stragglers, as observed in globular clusters (e.g., Benz & Hills 1987).

2.2. UV Emission

As in Sibony et al. (2022), we consider stars to radiate as black bodies and compute their average spectral luminosity $L_{*,\nu}(t)$ in a 100 \AA window around the typical rest-frame UV wavelength of 1500 \AA along their evolutionary tracks³. We then consider a mixed stellar population containing both CHE and non-rotating stars as a single-age starburst. This population is defined by two parameters, the mass fraction $f_{\text{CHE}} \in [0, 1]$ of CHE stars, and the minimal stellar mass $m_{*,\text{min}}^{\text{CHE}} \in [1.7, 20 M_\odot]$ for CHE to occur. For a given choice of $(f_{\text{CHE}}, m_{*,\text{min}}^{\text{CHE}})$, we first generate two stellar populations following a power-law IMF, $dN/dm_* \propto m_*^{-\alpha}$, with a slope of $\alpha = 2.35$ (Salpeter) or $\alpha = 1$ (top-heavy). The population of

CHE (non-rotating) stars is generated between $m_{*,\text{min}}^{\text{CHE}}$ ($m_{*,\text{min}} = 1.7 M_\odot$) and $m_{*,\text{max}} = 300 M_\odot$. For each population, we compute the total luminosity $L_\nu(t)$ by summing up the $L_{*,\nu}(t)$ for all stars that are still alive at time t , up to $t = 1 \text{ Gyr}$, which is then normalized by the total initial stellar mass M_* as $\mathcal{L}_\nu(t) \equiv L_\nu(t)/M_*$. Finally, we combine the CHE and non-rotating populations so that the mass fraction of CHE stars is f_{CHE} . For illustration, Figure 1 shows the resulting rest-frame UV light curves for $m_{*,\text{min}}^{\text{CHE}} = 1.7 M_\odot$ and varying f_{CHE} .

Note that in the aforementioned default model, the overall IMF of the mixed population is no longer a strict power-law when $f_{\text{CHE}} > 0$ and $m_{*,\text{min}}^{\text{CHE}} > m_{*,\text{min}} = 1.7 M_\odot$ as the CHE component is more top-heavy than the non-rotating component. An alternative approach is to turn a fraction of the stars above $m_{*,\text{min}}^{\text{CHE}}$ into CHE stars while keeping the overall IMF fixed to the chosen power-law form. In this case, the mass fraction of CHE stars has an upper limit $f_{\text{CHE}}^{\text{max}} = [\int_{m_{*,\text{min}}^{\text{CHE}}}^{m_{*,\text{max}}} m_* (dN/dm_*) dm_*] / [\int_{m_{*,\text{min}}}^{m_{*,\text{max}}} m_* (dN/dm_*) dm_*]$ as a function of $m_{*,\text{min}}^{\text{CHE}}$. Although we do not model this case explicitly, its outcomes can be estimated from the results of the default model via $f_{\text{CHE}}^{\text{max}}$, which do not change our conclusions made with the default model.

3. IMPACT ON FIRST GALAXY UV EMISSION

To predict the UV magnitudes of high- z galaxies and make direct comparisons with observations, we focus on the UV emission efficiency $\eta_{\text{UV}} \equiv \kappa_{\text{UV}}^{-1}$ defined as the

³ Using detailed stellar atmosphere models computed by the code TLUSTY (Hubeny 1988; Hubeny et al. 2021), we have verified that the relative errors in $L_{*,\nu}(t)$ introduced by the back-body assumption are within 30% for most CHE and non-rotating stars with $m_* \sim 3 - 300 M_\odot$, surface gravities $g \sim 10^{4.1-5.1} \text{ cm s}^{-2}$, and effective temperatures $T_{\text{eff}} \sim 10^{4.3} - 10^5 \text{ K}$, that dominate the overall rest-frame UV emission.

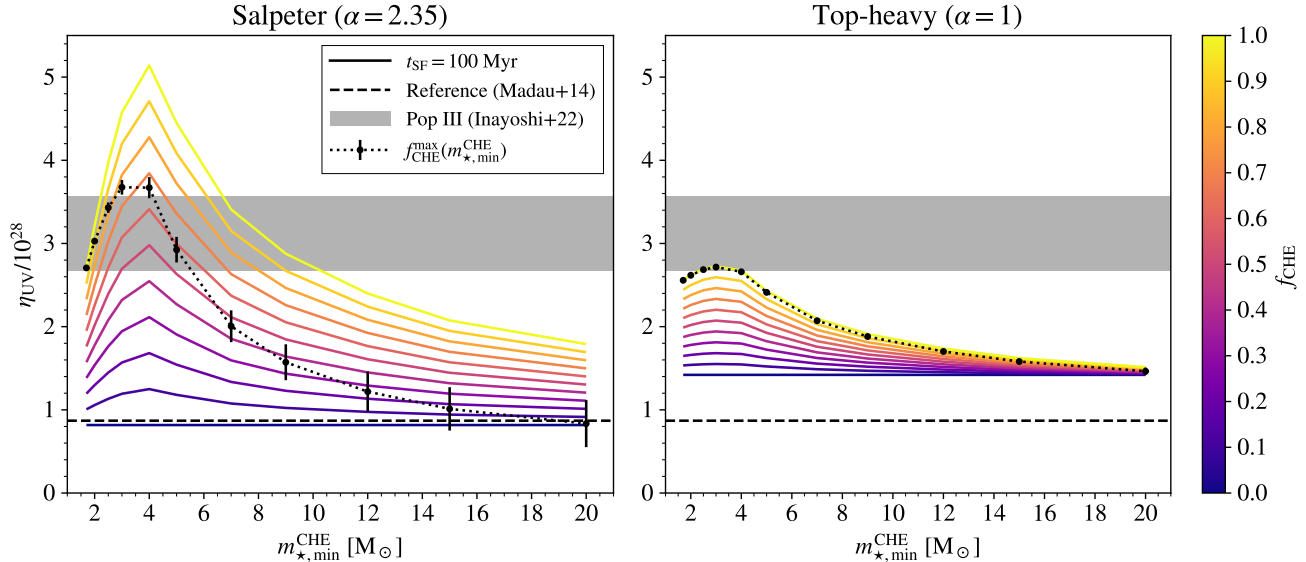


Figure 2. Rest-frame UV luminosity per unit SFE η_{UV} for a top-hat star formation history within a timescale $t_{SF} = 100$ Myr. As in Fig. 1, the left and right panel show the results for Salpeter and top-heavy IMFs, with $\alpha = 2.35$ and 1, respectively. While the mass range of normal stars is fixed as $m_{*} \in [1.7, 300] M_{\odot}$, we plot η_{UV} as a function of $m_{*,min}^{CHE}$ for $f_{CHE} \in [0, 1]$, where f_{CHE} increases for lighter colors (from bottom to top). The dotted curve with errorbars shows the maximum η_{UV} in the alternative population model with a fixed overall IMF (corresponding to the maximum CHE mass fraction f_{CHE}^{max}), which is estimated to be in between $\eta_{UV}(f_{CHE} = f_{CHE}^{max})$ and $f_{CHE}^{max}\eta_{UV}(f_{CHE} = 1)$. We also show the reference value $\eta_{UV} \simeq 8.70 \times 10^{27}$ from Madau & Dickinson (2014) with the dashed line, which is very close to our result for $f_{CHE} = 0$ given $\alpha = 2.35$. The shaded regions show the results for Pop III stars with extremely top-heavy IMFs from Inayoshi et al. (2022).

inverse of the conversion factor κ_{UV} between star formation rate (SFR) and rest-frame UV luminosity $L_{\nu}(UV)$:

$$\text{SFR}/(M_{\odot} \text{ yr}^{-1}) = \kappa_{UV} L_{\nu}(UV) / (\text{erg s}^{-1} \text{ Hz}^{-1}). \quad (1)$$

A reference value from local calibrations is $\eta_{UV} \simeq 8.70 \times 10^{27}$, corresponding to $\kappa_{UV} = 1.15 \times 10^{-28}$ (Madau & Dickinson 2014). Given the single-age starburst results (see Fig. 1), we calculate η_{UV} as a function of the CHE fraction f_{CHE} and minimum mass $m_{*,min}^{CHE}$ under different IMFs by integrating the stellar mass-normalized light curve $\mathcal{L}_{\nu}(t)$ over a simple top-hat star formation history with a constant SFR for a period of t_{SF} :

$$\eta_{UV} = \int_0^{t_{SF}} \mathcal{L}_{\nu}(t) dt \times M_{\odot} \text{ yr}^{-1} / (\text{erg s}^{-1} \text{ Hz}^{-1}). \quad (2)$$

We adopt $t_{SF} = 100$ Myr by default (see Appendix A for the results for $t_{SF} = 10$ and 1000 Myr) as the typical timescale of star formation probed by rest-frame UV emission, which is also close to the halo dynamical timescale and baryon cycle timescale at $z \sim 10$ (e.g., Anglés-Alcázar et al. 2017; Flores Velázquez et al. 2021; Tacchella et al. 2020). We have ignored the contribution of nebular emission and dust attenuation. It is shown in the Yggdrasil models (Zackrisson et al. 2011) that nebular emission in rest-frame UV is strongest for very

young star-forming clouds, reaching up to $\sim 40\%$ of the stellar luminosity in moderately metal-enriched environments with $Z \gtrsim 0.0004 \sim 0.03 Z_{\odot}$. However, it decays with time and becomes negligible ($\lesssim 10\%$ of the stellar contribution) shortly (\sim a few Myr $\ll t_{SF}$) after the starburst. Therefore, nebular emission is expected to be unimportant for the rest-frame UV emission of luminous high- z galaxies observable by *JWST*⁴. The effect of dust attenuation can be effectively absorbed into the UV variability parameter (see below and Shen et al. 2023).

The results are shown in Fig. 2. We obtain $\eta_{UV} \simeq 8.17 \times 10^{27}$ in the canonical case of Salpeter IMF without CHE ($f_{CHE} = 0$), which is very close to the reference value $\eta_{UV} \simeq 8.70 \times 10^{27}$ (Madau & Dickinson 2014). This further justifies our choice of $t_{SF} = 100$ Myr (as well as $m_{*,min} = 1.7 M_{\odot}$). Interestingly, the enhancement of UV emission by CHE peaks at $m_{*,min}^{CHE} =$

⁴ Nebular emission can dominate the rest-frame UV luminosity (reaching a few times of the stellar contribution) in the first few Myr after a starburst and remain comparable to stellar emission for up to ~ 20 Myr for pristine (metal-free) star-forming clouds hosting massive stars, if leakage of Lyman-continuum photons is not significant (Zackrisson et al. 2011). We do not consider such scenarios, since it is unclear whether the nebula can survive under strong radiative feedback and there is no confident detection of galaxies dominated by metal-free stellar populations.

4 (3) M_\odot for the Salpeter (top-heavy) IMF, reaching $\eta_{\text{UV}} \sim 5.14$ (2.73) $\times 10^{28}$ for $f_{\text{CHE}} = 1$, which is higher than the reference value by a factor of ~ 6 (3). Here, η_{UV} does not increase monotonically with $m_{\star,\text{min}}^{\text{CHE}}$ because the (lifetime-integrated) rest-frame UV emission is only boosted by CHE for $m_\star \lesssim 100 M_\odot$ but reduced for more massive stars. The latter become too hot under CHE, producing primarily more energetic (ionizing) photons (Sibony et al. 2022). For the same reason, the effect of CHE is generally stronger at $m_{\star,\text{min}}^{\text{CHE}} \lesssim 10 M_\odot$ when α or t_{SF} increase (see Appendix A) or with a smaller IMF upper mass limit $m_{\star,\text{max}}$. Without CHE, we obtain $\eta_{\text{UV}} = 1.42 \times 10^{28}$ under our top-heavy IMF (that extends down to $m_{\star,\text{min}} = 1.7 M_\odot$ with $\alpha = 1$), moderately increased by ~ 74 (63)% compared with the Salpeter (reference) case. It is shown in Inayoshi et al. (2022, see their table. 1) that considering extremely top-heavy IMFs ($m_\star \gtrsim 10 M_\odot$) for Pop III stars further increases the UV emission efficiency to $\eta_{\text{UV}} \sim 2.68 - 3.57 \times 10^{28}$ (see also Bromm et al. 2001). Comparable and higher values of η_{UV} can be achieved by CHE with $f_{\text{CHE}} \gtrsim 0.5$ and $m_{\star,\text{min}}^{\text{CHE}} \sim 2 - 10 M_\odot$ under a Salpeter IMF ($\alpha = 2.35$).

Given the results of $\eta_{\text{UV}}(f_{\text{CHE}})$ in the default model, the maximum UV efficiency in the alternative case of a fixed overall IMF should be in between $\eta_{\text{UV}}(f_{\text{CHE}} = f_{\text{CHE}}^{\text{max}})$ (with optimistic contributions from non-rotating stars below $m_{\star,\text{min}}^{\text{CHE}}$) and $f_{\text{CHE}}^{\text{max}} \eta_{\text{UV}}(f_{\text{CHE}} = 1)$ (ignoring non-rotating stars below $m_{\star,\text{min}}^{\text{CHE}}$). The resulting values are very close to $\eta_{\text{UV}}(f_{\text{CHE}} = 1)$ for the top-heavy IMF ($\alpha = 1$) as $f_{\text{CHE}}^{\text{max}} > 0.94$. For the Salpeter IMF with $f_{\text{CHE}}^{\text{max}} \sim 0.3 - 1$, the maximum UV emission efficiency peaks around $m_{\star,\text{min}}^{\text{CHE}} \sim 3 - 4 M_\odot$, reaching $\eta_{\text{UV}} \sim 3.6 - 3.8 \times 10^{28}$ given $f_{\text{CHE}}^{\text{max}} \sim 0.7 - 0.8$, which is still a factor of ~ 4 larger than the reference value.

Once η_{UV} is known, we derive the UV luminosity function (UVLF) using the model in Shen et al. (2023). First, we calculate the median UV magnitude M_{UV} as a function of halo mass M_{h} from the median SFR = $\epsilon_\star f_{\text{b}} \dot{M}_{\text{h}}$ estimated by the median halo accretion rate (Fakhouri et al. 2010)

$$\dot{M}_{\text{h}} \simeq 25.3 M_\odot \text{ yr}^{-1} \left(\frac{M_{\text{h}}}{10^{12} M_\odot} \right)^{1.1} \times (1 + 1.65z) \sqrt{\Omega_{\text{m}}(1+z)^3 + \Omega_{\Lambda}}, \quad (3)$$

and SFE (e.g., Tacchella et al. 2018; Harikane et al. 2022)

$$\epsilon_\star = \frac{2\epsilon_0}{(M_{\text{h}}/M_0)^{-\gamma} + (M_{\text{h}}/M_0)^\beta}. \quad (4)$$

Here $f_{\text{b}} \equiv \Omega_{\text{b}}/\Omega_{\text{m}} \simeq 0.16$ is the cosmic baryon fraction, and we adopt $\epsilon_0 = 0.1$, $\gamma = 0.6$, and $\beta = 0.5$ based

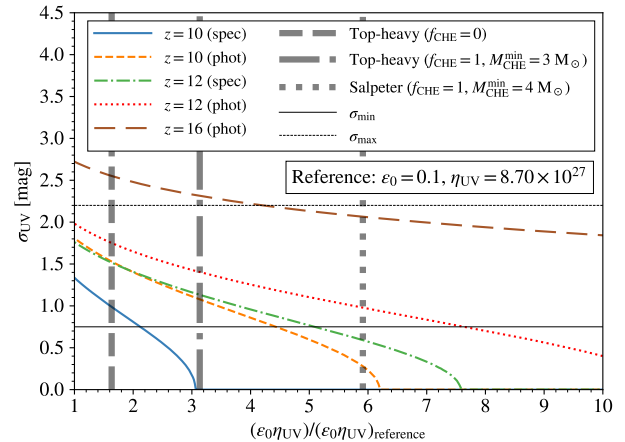


Figure 3. Constraints on UV emission efficiency and variability from *JWST* data. The colored curves show the values of $\epsilon_0 \eta_{\text{UV}}$ and σ_{UV} required to reproduce $\log(\Phi(M_{\text{UV}} = -20.5) [\text{mag}^{-1} \text{ cMpc}^{-3}]) = -5$ and -5.3 at $z = 10$ (solid) and 12 (dash-dotted) based on spectroscopy, and $\log(\Phi(M_{\text{UV}} = -20.5) [\text{mag}^{-1} \text{ cMpc}^{-3}]) = -4.5, -5,$ and -5.2 at $z = 10$ (dashed), 12 (dotted), and 16 (long dashed) from photometry. Three representative cases of different η_{UV} with fixed $\epsilon_0 = 0.1$ are shown by the thick vertical lines: the top-heavy models with no CHE ($f_{\text{CHE}} = 0$, dashed) and optimal CHE ($f_{\text{CHE}} = 1$, $m_{\star,\text{min}}^{\text{CHE}} = 3 M_\odot$, dash-dotted) and the Salpeter model with optimal CHE ($f_{\text{CHE}} = 1$, $m_{\star,\text{min}}^{\text{CHE}} = 4 M_\odot$, dotted). The thin solid and dashed horizontal lines show the minimum and maximum UV variability estimated by Shen et al. (2023).

on Behroozi et al. (2019, for the normalization and low-mass slope, matching the SFR- M_{h} relation at $z = 7$) and Harikane et al. (2022, for the high-mass slope). Next, this median $M_{\text{UV}}-M_{\text{h}}$ relation is combined with the halo mass function⁵ $dn/d \log M_{\text{h}}$ to derive the median UVLF $dn_{\text{median}}/dM_{\text{UV}} = (dn/d \log M_{\text{h}}) | \frac{d \log M_{\text{h}}}{dM_{\text{UV}}} |$, which is then convolved with a Gaussian kernel of width σ_{UV} (mag) to predict the observable UVLF $\Phi \equiv dn/dM_{\text{UV}}$. The last step captures the stochastic scatter in the scaling relations used above into the UV variability parameter σ_{UV} .

As illustrated in Shen et al. (2023, see their fig. 3), the UVLFs inferred from *JWST* observations place constraints on $\epsilon_0 \eta_{\text{UV}}$ and σ_{UV} , which can be estimated by considering the value of Φ at a typical magnitude $M_{\text{UV}} = -20.5$. Here, we require $\log(\Phi(M_{\text{UV}} =$

⁵ We use the HMF package (Murray et al. 2013) to calculate the halo mass function with the Tinker et al. (2010) model and real-space top-hat window function for a flat Λ CDM cosmology. The relevant cosmological parameters are based on Planck Collaboration et al. (2020) results: $H_0 = 67.66 \text{ km s}^{-1} \text{ Mpc}^{-1}$, $\Omega_{\text{m}} = 0.30966$, $n_{\text{s}} = 0.9667$, $\sigma_8 = 0.8159$, and $\Omega_{\text{b}} = 0.04897$.

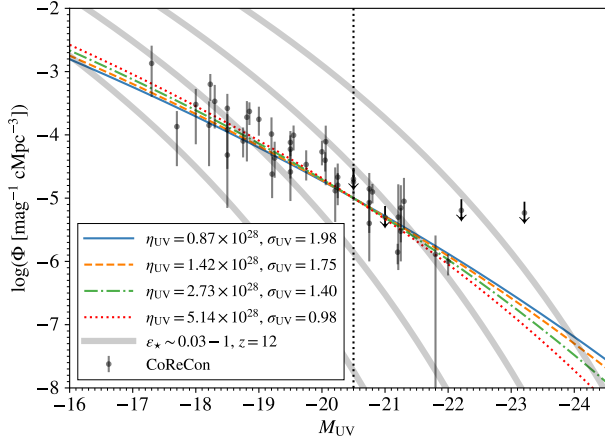


Figure 4. UVLF for select degenerate models that meet the photometric constraints from *JWST* at $z = 12$, i.e., $\log(\Phi(M_{\text{UV}} = -20.5) [\text{mag}^{-1} \text{cMpc}^{-3}]) = -5$. These include the reference case with $\eta_{\text{UV}} \simeq 8.70 \times 10^{27}$ (solid) and the three representative models with enhanced UV emission from CHE and/or a top-heavy IMF considered in Fig. 3. For comparison, the observational data for $z \sim 11 - 13$ (Naidu et al. 2022; Bouwens et al. 2023; Harikane et al. 2023; Pérez-González et al. 2023; Adams et al. 2024; Casey et al. 2024; Donnan et al. 2023, 2024; Finkelstein et al. 2024; McLeod et al. 2024; Robertson et al. 2024; Willott et al. 2024) are shown using CORECON (Garaldi 2023), among which the data points with arrows are upper limits. We also plot the results for constant SFE $\epsilon_* = 0.03, 0.1, 0.3$, and 1 (from bottom to top) without UV variability as the thick solid lines.

$-20.5) [\text{mag}^{-1} \text{cMpc}^{-3}] = -5$ and -5.3 at $z = 10$ and 12 according to spectroscopic observations, and $\log(\Phi(M_{\text{UV}} = -20.5) [\text{mag}^{-1} \text{cMpc}^{-3}]) = -4.5, -5$, and -5.2 at $z = 10, 12$, and 16 from photometric results, using the observational data compiled by the python package CORECON⁶ (Garaldi 2023). The corresponding values of $\epsilon_0 \eta_{\text{UV}}$ and σ_{UV} are shown in Fig. 3, where larger $\epsilon_0 \eta_{\text{UV}}$ and/or σ_{UV} are required to explain observations at higher z , and a smaller $\epsilon_0 \eta_{\text{UV}}$ can be compensated with a larger σ_{UV} .

To appreciate the trend and the degeneracy, we focus on 3 representative cases with boosted UV emission efficiency and fixed $\epsilon_0 = 0.1$: the top-heavy ($\alpha = 1$) models with no CHE ($f_{\text{CHE}} = 0$) and optimal CHE ($f_{\text{CHE}} = 1, m_{*,\text{min}}^{\text{CHE}} = 4 M_{\odot}$), and the Salpeter ($\alpha = 2.35$) model with optimal CHE ($f_{\text{CHE}} = 1, m_{*,\text{min}}^{\text{CHE}} = 3 M_{\odot}$). The corresponding UV variability parameters inferred from the photometric constraints at $z \sim 12$ (16) are $\sigma_{\text{UV}} = 1.75, 1.40$, and 0.98 (2.55, 2.31, and 2.06), respectively, while the reference value $\eta_{\text{UV}} \simeq 8.70 \times 10^{27}$

requires $\sigma_{\text{UV}} = 1.98$ (2.72). Clearly, with enhanced η_{UV} from CHE, smaller (less extreme) values of ϵ_0 and σ_{UV} are required to explain *JWST* results. In particular, only for the Salpeter model with optimal CHE ($f_{\text{CHE}} = 1, m_{*,\text{min}}^{\text{CHE}} = 3 M_{\odot}, \alpha = 2.35$) the σ_{UV} needed at $z \sim 16$ remains below the maximum value 2.2 estimated by Shen et al. (2023). Fig. 4 shows the UVLFs of the (degenerate) models at $z \sim 12$, which all agree well with current observations, but differ slightly in shape: The evolution of Φ with M_{UV} is stronger for larger (smaller) $\epsilon_0 \eta_{\text{UV}}$ (σ_{UV}), especially at the luminous end. Therefore, high precision measurements of UVLFs (in larger survey volumes) can potentially break the degeneracy between $\epsilon_0 \eta_{\text{UV}}$ and σ_{UV} . Additional constraints from galaxy clustering properties are also useful (Muñoz et al. 2023; Sun et al. 2024).

4. SUMMARY AND DISCUSSION

We explore the contribution of rapidly rotating stars under chemically homogeneous evolution (CHE) to the rest-frame UV ($\lambda \sim 1500 \text{ \AA}$) emission of the first galaxies. By incorporating CHE into a simple population synthesis model under the assumptions of black-body spectrum and negligible nebular emission, we predict the UV emission efficiency $\eta_{\text{UV}} \propto L_{\nu}(\text{UV})/\text{SFR}$ as a function of the mass fraction f_{CHE} and minimum mass $m_{*,\text{min}}^{\text{CHE}}$ of CHE stars with two power-law initial mass function (IMF) models ($dN/dm_* \propto m_*^{-\alpha}, \alpha = 2.35$ and 1). We then adopt the model in Shen et al. (2023) to calculate the relevant UV luminosity function (UVLF) and make comparisons with observations.

We find that CHE can significantly enhance the rest-frame UV emission of star-forming galaxies, as efficient as alternative scenarios of enhanced star formation efficiency and top-heavy IMFs. Compared with the canonical value from local calibrations (Madau & Dickinson 2014), η_{UV} is increased by a factor of $\sim 3 - 6$ for $f_{\text{CHE}} \gtrsim 0.5$ and $m_{*,\text{min}}^{\text{CHE}} \sim 2 - 10 M_{\odot}$ with a Salpeter IMF ($\alpha = 2.35, m_* < 300 M_{\odot}$) at the typical star-formation timescale $t_{\text{SF}} \sim 100 \text{ Myr}$. The effect of CHE is generally stronger for larger t_{SF} or IMF slope α . The enhanced UV emission from CHE can reproduce the UVLFs inferred from observations at $z \sim 12 - 16$ with less extreme values of star formation efficiency and stochastic variability of UV luminosity, within the range of current theoretical predictions.

In addition to boosting the UV emission (as well as ionizing power, see e.g., Sibony et al. 2022) of galaxies, populations of chemically homogeneous stars may have consequences for the nature of transients and for stellar nucleosynthesis. If homogeneous evolution is triggered by fast rotation, those stars (at least the massive ones)

⁶ <https://corecon.readthedocs.io/en/latest/index.html>

may produce long soft gamma ray bursts (GRBs), via the collapsar mechanism (e.g., Yoon & Langer 2005; Cantiello et al. 2007; Yoon et al. 2012). With the extension to high redshifts considered here, GRBs may then also originate in the first galaxies (e.g., Bromm & Loeb 2006), and their associated bright afterglows could act as background sources to probe the early intergalactic medium with absorption spectroscopy (Wang et al. 2012). The latter would be an ideal target for the upcoming suite of extremely large telescopes (ELTs). CHE may also play important roles in binary stellar evolution, regulating the properties of binary products, such as Wolf-Rayet stars, X-ray binaries, and binary black hole mergers (e.g., Mandel & de Mink 2016; de Mink & Mandel 2016; Marchant et al. 2017; du Buisson et al. 2020; Riley et al. 2021, Dall’Amico et al. in prep.). Moreover, those stars, if they lose mass, may enrich their surroundings in helium, hydrogen-burning products, and possibly also some helium-burning products,

while being depleted in lithium. This material could furthermore exhibit strong carbon over-abundances, thus leading to the formation of next-generation carbon-enhanced metal-poor stars (Liu et al. 2021; Jeena et al. 2023). All these aspects would deserve to be studied in future works, illustrating the various manifestations of rapid rotation in the early universe.

BL gratefully acknowledges funding from the Deutsche Forschungsgemeinschaft (DFG, German Research Foundation) under Germany’s Excellence Strategy EXC 2181/1 - 390900948 (the Heidelberg STRUCTURES Excellence Cluster). YS and GM have received funding from the European Research Council (ERC) under the European Union’s Horizon 2020 research and innovation programme (grant agreement No. 833925, project STAREX).

REFERENCES

- Adams, N. J., Conselice, C. J., Austin, D., et al. 2024, *ApJ*, 965, 169, doi: [10.3847/1538-4357/ad2a7b](https://doi.org/10.3847/1538-4357/ad2a7b)
- Anglés-Alcázar, D., Faucher-Giguère, C.-A., Kereš, D., et al. 2017, *MNRAS*, 470, 4698, doi: [10.1093/mnras/stx1517](https://doi.org/10.1093/mnras/stx1517)
- Behroozi, P., Wechsler, R. H., Hearin, A. P., & Conroy, C. 2019, *MNRAS*, 488, 3143, doi: [10.1093/mnras/stz1182](https://doi.org/10.1093/mnras/stz1182)
- Benz, W., & Hills, J. G. 1987, *ApJ*, 323, 614, doi: [10.1086/165857](https://doi.org/10.1086/165857)
- Bouwens, R. J., Stefanon, M., Brammer, G., et al. 2023, *MNRAS*, 523, 1036, doi: [10.1093/mnras/stad1145](https://doi.org/10.1093/mnras/stad1145)
- Boylan-Kolchin, M. 2023, *Nature Astronomy*, 7, 731, doi: [10.1038/s41550-023-01937-7](https://doi.org/10.1038/s41550-023-01937-7)
- Bromm, V., Kudritzki, R. P., & Loeb, A. 2001, *ApJ*, 552, 464, doi: [10.1086/320549](https://doi.org/10.1086/320549)
- Bromm, V., & Loeb, A. 2006, *ApJ*, 642, 382, doi: [10.1086/500799](https://doi.org/10.1086/500799)
- Bunker, A. J., Saxena, A., Cameron, A. J., et al. 2023, *A&A*, 677, A88, doi: [10.1051/0004-6361/202346159](https://doi.org/10.1051/0004-6361/202346159)
- Cantiello, M., Yoon, S. C., Langer, N., & Livio, M. 2007, *A&A*, 465, L29, doi: [10.1051/0004-6361:20077115](https://doi.org/10.1051/0004-6361:20077115)
- Casey, C. M., Akins, H. B., Shuntov, M., et al. 2024, *ApJ*, 965, 98, doi: [10.3847/1538-4357/ad2075](https://doi.org/10.3847/1538-4357/ad2075)
- Cueto, E. R., Hutter, A., Dayal, P., et al. 2024, *A&A*, 686, A138, doi: [10.1051/0004-6361/202349017](https://doi.org/10.1051/0004-6361/202349017)
- de Mink, S. E., & Mandel, I. 2016, *MNRAS*, 460, 3545, doi: [10.1093/mnras/stw1219](https://doi.org/10.1093/mnras/stw1219)
- Dekel, A., Sarkar, K. C., Birnboim, Y., Mandelker, N., & Li, Z. 2023, *MNRAS*, 523, 3201, doi: [10.1093/mnras/stad1557](https://doi.org/10.1093/mnras/stad1557)
- D’Eugenio, F., Maiolino, R., Carniani, S., et al. 2024, *A&A*, 689, A152, doi: [10.1051/0004-6361/202348636](https://doi.org/10.1051/0004-6361/202348636)
- Donnan, C. T., McLeod, D. J., McLure, R. J., et al. 2023, *MNRAS*, 520, 4554, doi: [10.1093/mnras/stad471](https://doi.org/10.1093/mnras/stad471)
- Donnan, C. T., McLure, R. J., Dunlop, J. S., et al. 2024, *MNRAS*, 533, 3222, doi: [10.1093/mnras/stae2037](https://doi.org/10.1093/mnras/stae2037)
- du Buisson, L., Marchant, P., Podsiadlowski, P., et al. 2020, *MNRAS*, 499, 5941, doi: [10.1093/mnras/staa3225](https://doi.org/10.1093/mnras/staa3225)
- Fakhouri, O., Ma, C.-P., & Boylan-Kolchin, M. 2010, *MNRAS*, 406, 2267, doi: [10.1111/j.1365-2966.2010.16859.x](https://doi.org/10.1111/j.1365-2966.2010.16859.x)
- Ferrara, A. 2024, *A&A*, 689, A310, doi: [10.1051/0004-6361/202450944](https://doi.org/10.1051/0004-6361/202450944)
- Finkelstein, S. L., Bagley, M. B., Ferguson, H. C., et al. 2023, *ApJL*, 946, L13, doi: [10.3847/2041-8213/acade4](https://doi.org/10.3847/2041-8213/acade4)
- Finkelstein, S. L., Leung, G. C. K., Bagley, M. B., et al. 2024, *ApJL*, 969, L2, doi: [10.3847/2041-8213/ad4495](https://doi.org/10.3847/2041-8213/ad4495)
- Flores Velázquez, J. A., Gurvich, A. B., Faucher-Giguère, C.-A., et al. 2021, *MNRAS*, 501, 4812, doi: [10.1093/mnras/staa3893](https://doi.org/10.1093/mnras/staa3893)
- Garaldi, E. 2023, *The Journal of Open Source Software*, 8, 5407, doi: [10.21105/joss.05407](https://doi.org/10.21105/joss.05407)
- Gormaz-Matamala, A. C., Cuadra, J., Ekström, S., et al. 2024, *A&A*, 687, A290, doi: [10.1051/0004-6361/202449782](https://doi.org/10.1051/0004-6361/202449782)

- Harikane, Y., Ouchi, M., Oguri, M., et al. 2022, arXiv e-prints, arXiv:2208.01612.
<https://arxiv.org/abs/2208.01612>
- . 2023, *ApJS*, 265, 5, doi: [10.3847/1538-4365/aca9a9](https://doi.org/10.3847/1538-4365/aca9a9)
- Hirano, S., & Bromm, V. 2018, *MNRAS*, 476, 3964, doi: [10.1093/mnras/sty487](https://doi.org/10.1093/mnras/sty487)
- Hubeny, I. 1988, *Computer Physics Communications*, 52, 103, doi: [10.1016/0010-4655\(88\)90177-4](https://doi.org/10.1016/0010-4655(88)90177-4)
- Hubeny, I., Allende Prieto, C., Osorio, Y., & Lanz, T. 2021, arXiv e-prints, arXiv:2104.02829, doi: [10.48550/arXiv.2104.02829](https://doi.org/10.48550/arXiv.2104.02829)
- Inayoshi, K., Harikane, Y., Inoue, A. K., Li, W., & Ho, L. C. 2022, *ApJL*, 938, L10, doi: [10.3847/2041-8213/ac9310](https://doi.org/10.3847/2041-8213/ac9310)
- Jeena, S. K., Banerjee, P., Chiaki, G., & Heger, A. 2023, *MNRAS*, 526, 4467, doi: [10.1093/mnras/stad3028](https://doi.org/10.1093/mnras/stad3028)
- Jeong, T. B., Jeon, M., Song, H., & Bromm, V. 2024, arXiv e-prints, arXiv:2411.17007, doi: [10.48550/arXiv.2411.17007](https://doi.org/10.48550/arXiv.2411.17007)
- Kroupa, P. 2001, *MNRAS*, 322, 231, doi: [10.1046/j.1365-8711.2001.04022.x](https://doi.org/10.1046/j.1365-8711.2001.04022.x)
- Labbé, I., van Dokkum, P., Nelson, E., et al. 2023, *Nature*, 616, 266, doi: [10.1038/s41586-023-05786-2](https://doi.org/10.1038/s41586-023-05786-2)
- Liu, B., & Bromm, V. 2022, *ApJL*, 937, L30, doi: [10.3847/2041-8213/ac927f](https://doi.org/10.3847/2041-8213/ac927f)
- Liu, B., Gurian, J., Inayoshi, K., et al. 2024, *MNRAS*, 534, 290, doi: [10.1093/mnras/stae2066](https://doi.org/10.1093/mnras/stae2066)
- Liu, B., Sibony, Y., Meynet, G., & Bromm, V. 2021, *MNRAS*, 506, 5247, doi: [10.1093/mnras/stab2057](https://doi.org/10.1093/mnras/stab2057)
- Madau, P., & Dickinson, M. 2014, *ARA&A*, 52, 415, doi: [10.1146/annurev-astro-081811-125615](https://doi.org/10.1146/annurev-astro-081811-125615)
- Maeder, A. 1987, *A&A*, 178, 159
- Maeder, A., & Meynet, G. 2000, *ARA&A*, 38, 143, doi: [10.1146/annurev.astro.38.1.143](https://doi.org/10.1146/annurev.astro.38.1.143)
- . 2012, *Reviews of Modern Physics*, 84, 25, doi: [10.1103/RevModPhys.84.25](https://doi.org/10.1103/RevModPhys.84.25)
- Mandel, I., & de Mink, S. E. 2016, *MNRAS*, 458, 2634, doi: [10.1093/mnras/stw379](https://doi.org/10.1093/mnras/stw379)
- Marchant, P., Langer, N., Podsiadlowski, P., et al. 2017, *A&A*, 604, A55, doi: [10.1051/0004-6361/201630188](https://doi.org/10.1051/0004-6361/201630188)
- McLeod, D. J., Donnan, C. T., McLure, R. J., et al. 2024, *MNRAS*, 527, 5004, doi: [10.1093/mnras/stad3471](https://doi.org/10.1093/mnras/stad3471)
- Muñoz, J. B., Mirocha, J., Furlanetto, S., & Sabti, N. 2023, *MNRAS*, 526, L47, doi: [10.1093/mnras/sladd115](https://doi.org/10.1093/mnras/sladd115)
- Murphy, L. J., Groh, J. H., Ekström, S., et al. 2021, *MNRAS*, 501, 2745, doi: [10.1093/mnras/staa3803](https://doi.org/10.1093/mnras/staa3803)
- Murray, S. G., Power, C., & Robotham, A. S. G. 2013, *Astronomy and Computing*, 3, 23, doi: [10.1016/j.ascom.2013.11.001](https://doi.org/10.1016/j.ascom.2013.11.001)
- Naidu, R. P., Oesch, P. A., van Dokkum, P., et al. 2022, *ApJL*, 940, L14, doi: [10.3847/2041-8213/ac9b22](https://doi.org/10.3847/2041-8213/ac9b22)
- Nandal, D., Sibony, Y., & Tsiatsiou, S. 2024, *A&A*, 688, A142, doi: [10.1051/0004-6361/202348866](https://doi.org/10.1051/0004-6361/202348866)
- Pérez-González, P. G., Costantin, L., Langeroodi, D., et al. 2023, *ApJL*, 951, L1, doi: [10.3847/2041-8213/acd9d0](https://doi.org/10.3847/2041-8213/acd9d0)
- Planck Collaboration, Aghanim, N., Akrami, Y., et al. 2020, *A&A*, 641, A6, doi: [10.1051/0004-6361/201833910](https://doi.org/10.1051/0004-6361/201833910)
- Riley, J., Mandel, I., Marchant, P., et al. 2021, *MNRAS*, 505, 663, doi: [10.1093/mnras/stab1291](https://doi.org/10.1093/mnras/stab1291)
- Robertson, B., Johnson, B. D., Tacchella, S., et al. 2024, *ApJ*, 970, 31, doi: [10.3847/1538-4357/ad463d](https://doi.org/10.3847/1538-4357/ad463d)
- Shen, X., Vogelsberger, M., Boylan-Kolchin, M., Tacchella, S., & Kannan, R. 2023, *MNRAS*, 525, 3254, doi: [10.1093/mnras/stad2508](https://doi.org/10.1093/mnras/stad2508)
- Shen, X., Vogelsberger, M., Boylan-Kolchin, M., Tacchella, S., & Naidu, R. P. 2024, *MNRAS*, 533, 3923, doi: [10.1093/mnras/stae1932](https://doi.org/10.1093/mnras/stae1932)
- Sibony, Y., Liu, B., Simmonds, C., Meynet, G., & Bromm, V. 2022, *A&A*, 666, A199, doi: [10.1051/0004-6361/202244146](https://doi.org/10.1051/0004-6361/202244146)
- Song, H. F., Meynet, G., Maeder, A., Ekström, S., & Eggenberger, P. 2016, *A&A*, 585, A120, doi: [10.1051/0004-6361/201526074](https://doi.org/10.1051/0004-6361/201526074)
- Stacy, A., Bromm, V., & Loeb, A. 2011, *MNRAS*, 413, 543, doi: [10.1111/j.1365-2966.2010.18152.x](https://doi.org/10.1111/j.1365-2966.2010.18152.x)
- Stacy, A., Greif, T. H., Klessen, R. S., Bromm, V., & Loeb, A. 2013, *MNRAS*, 431, 1470, doi: [10.1093/mnras/stt264](https://doi.org/10.1093/mnras/stt264)
- Sun, G., Muñoz, J. B., Mirocha, J., & Faucher-Giguère, C.-A. 2024, arXiv e-prints, arXiv:2410.21409, doi: [10.48550/arXiv.2410.21409](https://doi.org/10.48550/arXiv.2410.21409)
- Tacchella, S., Bose, S., Conroy, C., Eisenstein, D. J., & Johnson, B. D. 2018, *ApJ*, 868, 92, doi: [10.3847/1538-4357/aae8e0](https://doi.org/10.3847/1538-4357/aae8e0)
- Tacchella, S., Forbes, J. C., & Caplar, N. 2020, *MNRAS*, 497, 698, doi: [10.1093/mnras/staa1838](https://doi.org/10.1093/mnras/staa1838)
- Telford, O. G., Chisholm, J., Sander, A. A. C., et al. 2024, *ApJ*, 974, 85, doi: [10.3847/1538-4357/ad697e](https://doi.org/10.3847/1538-4357/ad697e)
- Tinker, J. L., Robertson, B. E., Kravtsov, A. V., et al. 2010, *ApJ*, 724, 878, doi: [10.1088/0004-637X/724/2/878](https://doi.org/10.1088/0004-637X/724/2/878)
- Topping, M. W., Stark, D. P., Senchyna, P., et al. 2024, *MNRAS*, 529, 3301, doi: [10.1093/mnras/stae682](https://doi.org/10.1093/mnras/stae682)
- Trinca, A., Schneider, R., Valiante, R., et al. 2024, *MNRAS*, 529, 3563, doi: [10.1093/mnras/stae651](https://doi.org/10.1093/mnras/stae651)
- Tsiatsiou, S., Sibony, Y., Nandal, D., et al. 2024, *A&A*, 687, A307, doi: [10.1051/0004-6361/202449156](https://doi.org/10.1051/0004-6361/202449156)
- Ventura, E. M., Qin, Y., Balu, S., & Wyithe, J. S. B. 2024, *MNRAS*, 529, 628, doi: [10.1093/mnras/stae567](https://doi.org/10.1093/mnras/stae567)
- Vink, J. S., de Koter, A., & Lamers, H. J. G. L. M. 2001, *A&A*, 369, 574, doi: [10.1051/0004-6361:20010127](https://doi.org/10.1051/0004-6361:20010127)

Wang, F. Y., Bromm, V., Greif, T. H., et al. 2012, ApJ, 760, 27, doi: [10.1088/0004-637X/760/1/27](https://doi.org/10.1088/0004-637X/760/1/27)

Willott, C. J., Desprez, G., Asada, Y., et al. 2024, ApJ, 966, 74, doi: [10.3847/1538-4357/ad35bc](https://doi.org/10.3847/1538-4357/ad35bc)

Yoon, S. C., Dierks, A., & Langer, N. 2012, A&A, 542, A113, doi: [10.1051/0004-6361/201117769](https://doi.org/10.1051/0004-6361/201117769)

Yoon, S. C., & Langer, N. 2005, A&A, 443, 643, doi: [10.1051/0004-6361:20054030](https://doi.org/10.1051/0004-6361:20054030)

Zackrisson, E., Rydberg, C.-E., Schaerer, D., Östlin, G., & Tuli, M. 2011, ApJ, 740, 13, doi: [10.1088/0004-637X/740/1/13](https://doi.org/10.1088/0004-637X/740/1/13)

Zepeda, J., Beers, T. C., Placco, V. M., et al. 2023, ApJ, 947, 23, doi: [10.3847/1538-4357/acbbcc](https://doi.org/10.3847/1538-4357/acbbcc)

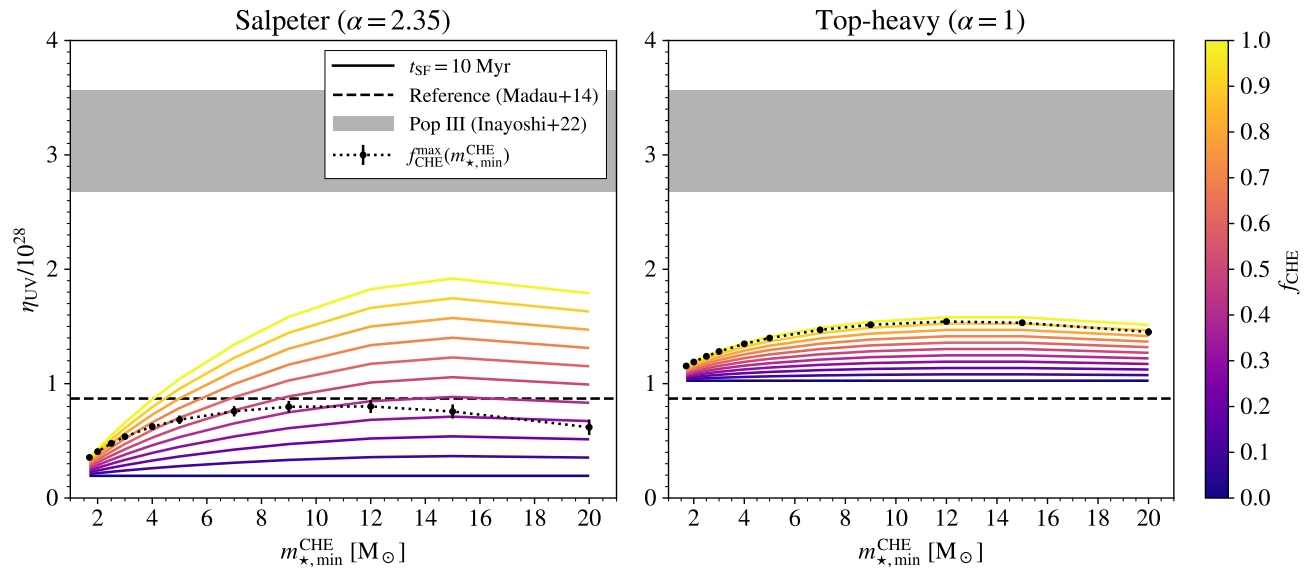


Figure 5. Same as Fig. 2 but for a star-formation timescale $t_{\text{SF}} = 10$ Myr.

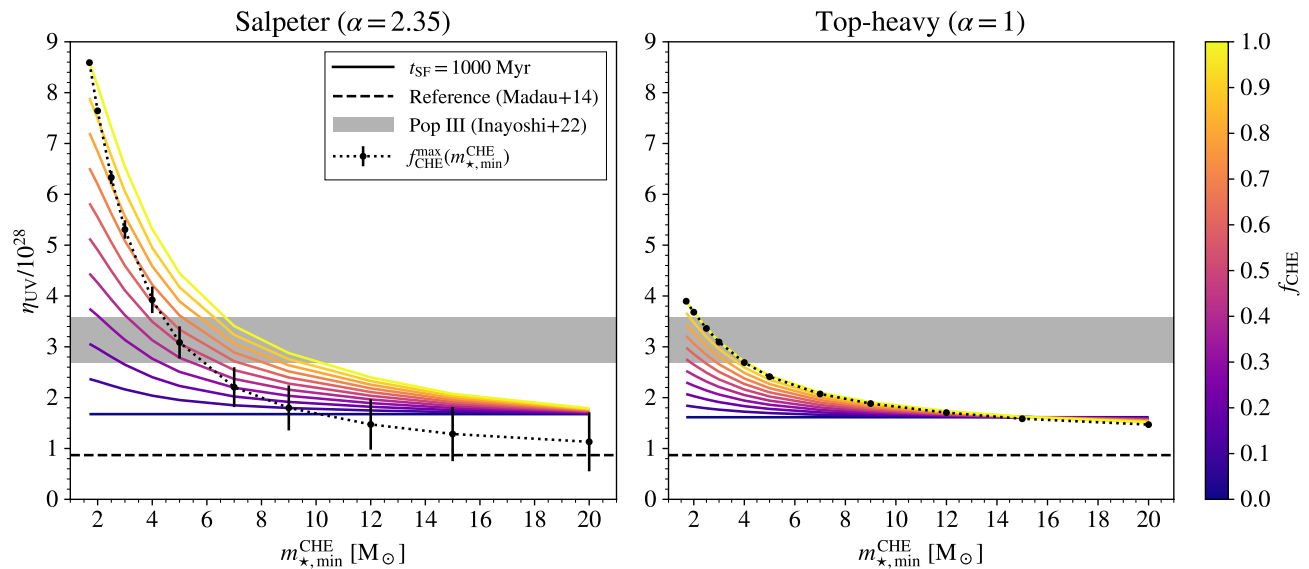


Figure 6. Same as Fig. 2 but for a star-formation timescale $t_{\text{SF}} = 1000$ Myr.

APPENDIX

A. SFR-UV CONVERSION FACTORS FOR DIFFERENT STAR-FORMATION TIMESCALES